Electron Raman scattering in a cylindrical quantum dot

Zhong Qinghu(钟庆湖)† and Yi Xuehua(易学华)

Department of Physics and Optical Information Sciences, Jiaying University, Meizhou 514015, China

Abstract: Electron Raman scattering (ERS) is investigated in a CdS cylindrical quantum dot (QD). The differential cross section is calculated as a function of the scattering frequency and the size of the QD. Single parabolic conduction and valence bands are assumed, and singularities in the spectrum are found and interpreted. The selection rules for the processes are also studied. The ERS studied here can be used to provide direct information about the electron band structure of these systems.

Key words: electron Raman scattering; quantum dot; differential cross-section; selection rule
DOI: 10.1088/1674-4926/33/5/052001 **EEACC:** 2570

1. Introduction

Low-dimensional semiconductor systems, such as quantum wells (QWs), quantum wires and quantum dots (QDs), have attracted considerable attention because they show many special physical properties associated with quantum confinement effects, and have many applications in the opto-electronic and microelectronic fields[1−3]. With the progress in semiconductor nanotechnology, such as molecular-beam epitaxy and metal-organic chemical-vapor deposition, various kinds of semiconductor heterostructures can be fabricated. Furthermore, studies reveal that the peculiar properties of QD behavior strongly differ from those of one-dimensional and two-dimensional systems. It was suggested as early as 1982 that lasers based on QD structures should exhibit superior performance compared with those based on quantum wires and QWs due to a noticeable modification of the density of states[4]. Furthermore, many new devices such as quantum transistors, high-speed memory elements, narrowband high-emitting diodes and infrared photodetectors, which are based on QDs, are found to have more advantages than those based on quantum wires and QWs[5, 6].

Electron Raman scattering (ERS) is a powerful tool for providing direct information on the energy band structure and different physical properties of semiconductor nanostructure systems[7−9]. In particular, the electronic structure of semiconductor materials and nanostructures can be thoroughly investigated considering different polarizations for the incident and emitted radiation[10]. Experimental research on Raman scattering in nanocrystals has been extensively reported. Many theoretical studies that attempt to interpret experimental results usually focus on the calculation of the differential cross section (DCS) for Raman scattering[11−14]. Thus, the calculation of the DCS remains a piece of fundamental work.

Multiphonon or one-phonon assisted Raman scattering has been discussed for many nanostructures[15]. Meanwhile, Raman scattering without involving phonons has also been reported, and the rich spectra which are the main characteristic of the ERS have been observed[16]. In this paper, we calculated the DCS of ERS due to the electron and hole without the assistance of the phonons in a QD system under various QD sizes. Due to the anisotropic optical activity in low-dimensional semiconductors[17, 18], we found that as the QD size decreases, the DCS increases. We obtained the rich ERS spectra, which provide direct information about the electron band structure of these systems. Dielectric and quantum confinement effects result in prominent exciton features such as large binding energies and oscillator strengths[19]. In our paper, we find that quantum confinement effects can also intensify the DCS of Raman scattering.

2. Model and theory

Let us briefly describe the model and fundamental theory applied in our calculations. We consider a cylindrical QD with infinite potential barriers. The radius and the height of the QD are R and $2d$, respectively. As explained above, we consider a single conduction (valence) band, which splits into a subband system due to complete electron confinement within the QD. In the envelope function approximation, neglecting the electron–hole Coulomb interaction, the solution of the Schrödinger equation in a conduction band can be written as

$$\psi_{m_e,t_e,l_e} = \frac{1}{J_{m_e+1}(\chi_{m_e t_e})R\sqrt{\pi d}} J_{m_e}\left(\frac{\chi_{m_e t_e}}{R} r\right) \times \sin\frac{l_e \pi (z+d)}{2d} e^{i m_e \varphi} u_e, \quad (1)$$

where J_{m_e} and J_{m_e+1} are the m_eth-order and (m_e+1)th-order Bessel function; $l_e = 1, 2, 3, \ldots$ is the quantum number related to the projection of the angular momentum on the z-direction; u_e is the Bloch function taken at $\boldsymbol{k}_0$, where (by assumption) the band extrema are located; and $\chi_{m_e t_e}$ is the t_eth zero of the m_eth-order Bessel function, i.e. $J_{m_e}(\chi_{m_e l_e}) = 0$.

The energy eigenvalues in the conduction band are given by

$$E_{m_e t_e l_e} = \frac{\hbar}{2m_e^*}\left[\left(\frac{\chi_{m_e t_e}}{R}\right)^2 + \left(\frac{l_e \pi}{2d}\right)^2\right] + E_g, \quad (2)$$

† Corresponding author. Email: qhzhong05@163.com
Received 29 September 2011, revised manuscript received 13 November 2011

where m_e^* is the effective mass of an electron and E_g is the energy gap between the valence and conduction bands.

Similarly, the wave function and energy eigenvalues for the holes in the valence band are as follows:

$$\psi_{m_h, t_h, l_h} = \frac{1}{J_{m_h+1}(\chi_{m_h t_h}) R\sqrt{\pi d}} \times J_{m_h}\left(\frac{\chi_{m_h t_h}}{R} r\right) \sin\frac{l_h \pi (z+d)}{2d} e^{i m_h \varphi} u_h, \quad (3)$$

$$E_{m_h t_h l_h} = \frac{\hbar}{2m_h^*}\left[\left(\frac{\chi_{m_h t_h}}{R}\right)^2 + \left(\frac{l_h \pi}{2d}\right)^2\right], \quad (4)$$

where m_h^* is the effective mass of a hole.

3. The differential cross-section

The general expression for the ERS differential cross-section is given by the following equation[11]:

$$\frac{d^2\sigma}{d\Omega d\omega_s} = \frac{v^2 \omega_s^2 \eta(\omega_s)}{8\pi^3 c^4 \eta(\omega_l)} W(\omega_s, \boldsymbol{e}_s), \quad (5)$$

where c is the light velocity in vacuum, $\eta(\omega)$ is the refraction index as a function of the radiation frequency, $\boldsymbol{e}_s$ is the polarization vector for the emitted secondary radiation field, v is the normalization volume, ω_s is the secondary radiation frequency, and ω_l is the frequency of the incident radiation. $W(\omega_s, \boldsymbol{e}_s)$ is the transition rate calculated according to

$$W(\omega_s, \boldsymbol{e}_s) = \frac{2\pi}{\hbar} \sum_f |M_e + M_h|^2 \delta(E_f - E_i), \quad (6)$$

where

$$M_j = \sum_a \frac{\langle f | H_{js} | a\rangle \langle a | H_l | i\rangle}{E_i - E_a + i\Gamma_a} + \sum_b \frac{\langle f | H_l | b\rangle \langle b | H_{js} | i\rangle}{E_i - E_b + i\Gamma_b}. \quad (7)$$

In Eq. (7) $j = e, h$ are for the cases of electrons or holes, respectively, and $|i\rangle$ and $|f\rangle$ denote the initial and final states of the system with their corresponding energies E_i and E_f. $|a\rangle$ and $|b\rangle$ are intermediate states with energies E_a and E_b. Γ_a and Γ_b are the lifetime broadenings in the intermediated states.

The operator H_l is of the form

$$\hat{H}_l = \frac{e}{m_0}\sqrt{\frac{2\pi\hbar}{V\omega_l}} \boldsymbol{e}_l \cdot \hat{\boldsymbol{p}}, \quad \hat{\boldsymbol{p}} = -i\hbar\nabla, \quad (8)$$

where m_0 is the free electron mass. This operator describes the interaction with the incident radiation field in the dipole approximation. The interaction with the secondary radiation field is described by the operator

$$\hat{H}_{js} = \frac{e}{m_j^*}\sqrt{\frac{2\pi\hbar}{V\omega_s}} \boldsymbol{e}_{js} \cdot \hat{\boldsymbol{p}}, \quad j = e, h. \quad (9)$$

This Hamiltonian describes the photon emission by the electron (hole) after the transition between the conduction (valence) subbands of the system.

In the initial state $|i\rangle$ there is an incident radiation photon with energy $\hbar\omega_l$; the conduction band is considered to be empty and the valence band is completely occupied by the electron. The energy of the initial state is

$$E_i = \hbar\omega_l. \quad (10)$$

The final state of the process involves an EHP in a real state and a scattered light with energy $\hbar\omega_s$. Thus,

$$E_f = \hbar\omega_s + E_{m_e l_e t_e} + E_{m_h l_h t_h} + E_g, \quad (11)$$

where $E_{m_e l_e t_e}$ and $E_{m_h l_h t_h}$ are determined by Eq. (2) and (4). Using the energy conservation law we get

$$E_i - E_a = E_{m_e l_e t_e} - E_{m'_e l'_e t'_e} + \hbar\omega_s, \quad (12)$$

for the electron intermediate states and

$$E_i - E_b = E_{m'_h l'_h t'_h} - E_{m_h l_h t_h} - \hbar\omega_s, \quad (13)$$

for the hole intermediate states.

In the following, we calculate the matrix elements of the DCS in the scattering configurations $Z(\boldsymbol{e}_l, \boldsymbol{e}_{s\rho})\overline{Z}$.

$$\langle a | \hat{H}_l | i\rangle = \frac{i m_{1e}^* |e|}{m_0}\sqrt{\frac{2\pi}{v\hbar\omega_l}} \frac{2W_{t_h t'_e}}{J_{m_h+1}(\chi_{m_h t_h}) J_{m'_e+1}(\chi_{m'_e t'_e}) R^2} \times \Gamma_1 \delta_{m_h m'_e} \delta_{l_h l'_e}, \quad (14)$$

$$\langle b | \hat{H}_s | i\rangle = i|e|\sqrt{\frac{2\pi}{v\hbar\omega_s}} \frac{2W_{t_e t'_e}}{J_{m_e+1}(\chi_{m_e t_e}) J_{m'_e+1}(\chi_{m'_e t'_e}) R^2} \times \Gamma_2 \delta_{m_e m'_e} \delta_{l_h l'_e}, \quad (15)$$

where

$$\Gamma_1 = \int_0^R J_{m_h}\left(\frac{\chi_{m_h t_h}}{R} r\right) J_{m'_e}\left(\frac{\chi_{l'_e t'_e}}{R} r\right) r^2 dr, \quad (16)$$

$$\Gamma_2 = \int_0^R J_{m_e}\left(\frac{\chi_{m_e t_e}}{R} r\right) J_{m'_e}\left(\frac{\chi_{l'_e t'_e}}{R} r\right) r^2 dr, \quad (17)$$

$$W_{t_h t'_e} = E_{m'_e l'_e t'_e} - E_{m_h l_h t_h} \quad (18)$$

$$W_{t'_e t_e} = E_{m'_e l'_e t'_e} - E_{m_e l_e t_e} \quad (19)$$

After a tedious calculation, the DCS for the intermediate states in the conduction band can be written as,

$$\left[\frac{d^2\sigma}{d\Omega d\omega_s}\right]_e = \frac{16 m_e^{*2} e^4 \omega_s \eta(\omega_s)}{m_0^2 c^4 \hbar^3 R^8 \omega_l \eta(\omega_l)} \frac{1}{(E_e - E_a)^2 + \Gamma_a^2} \times \left| \frac{W_{t_h t'_e} W_{t'_e t_e}}{J_{m_h+1}(\chi_{m_h t_h}) J^2_{m'_e+1}(\chi_{m'_e t'_e}) J_{m_e+1}(\chi_{m_e t_e})} \Gamma_1 \Gamma_2 \right|^2. \quad (20)$$

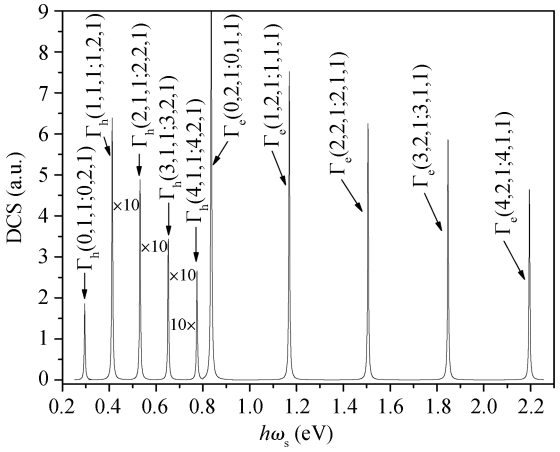

Fig. 1. Raman spectrum of the CdS cylindrical QD in the scattering configuration $Z(\boldsymbol{e}_1, \boldsymbol{e}_{\rm sr})\overline{Z}$. The radius and thickness are 2.5 and 3.0 nm.

We can get similar expressions for the interband ERS process with the intermediate states in the valence band (with replacements $m_{\rm e} \to m'_{\rm h}, m'_{\rm e} \to m_{\rm h}, l_{\rm e} \to l'_{\rm h}, l'_{\rm e} \to l_{\rm h}$, $t_{\rm e} \to t'_{\rm h}, t'_{\rm e} \to t_{\rm h}$ and $m^*_{\rm e} \to m^*_{\rm h}$):

$$\left[\frac{{\rm d}^2\sigma}{{\rm d}\Omega{\rm d}\omega_{\rm s}}\right]_{\rm h} = \frac{16m^{*2}_{\rm h}e^4\omega_{\rm s}\eta(\omega_{\rm s})}{m_0^2c^4\hbar^3R^8\omega_{\rm l}\eta(\omega_{\rm l})} \quad \frac{1}{(E_{\rm e}-E_{\rm a})^2+\Gamma_{\rm a}^2} \times \left|\frac{W_{t'_{\rm h}t_{\rm e}}W_{t_{\rm h}t'_{\rm h}}}{J_{m_{\rm h}+1}(\chi_{m_{\rm h}t_{\rm h}})J^2_{m'_{\rm h}+1}(\chi_{m'_{\rm h}t'_{\rm h}})J_{m_{\rm e}+1}(\chi_{m_{\rm e}t_{\rm e}})}\Gamma_1\Gamma_2\right|^2. \tag{21}$$

From Eqs. (14) and (15), it is clearly seen that the following selection rules must be satisfied if the DCS is not equal to zero:

$$\begin{aligned} &l_{\rm h} = l'_{\rm e} = l_{\rm e}, \quad m_{\rm h} = m'_{\rm e} = m_{\rm e}, \qquad j = {\rm e}, \\ &l_{\rm e} = l'_{\rm h} = l_{\rm h}, \quad m_{\rm e} = m'_{\rm h} = m_{\rm h}, \qquad j = {\rm h}. \end{aligned} \tag{22}$$

4. Results and discussion

In this section, we present the numerical calculations of the DCS for ERS in the CdS cylindrical QD. The physical parameters used in our expression are[20]: $m^*_{\rm e} = 0.18m_0$, $m^*_{\rm h} = 0.51m_0$, $E_{\rm g} = 3.9$ eV and $\Gamma_{\rm a} = \Gamma_{\rm b} = 1$ meV.

From Eqs. (20) and (21), it is easy to find that the emission spectrum show maximums at the following values of $\omega_{\rm s}$,

$$\omega_{\rm s} = \frac{1}{\hbar}(E_{m'_{\rm e}l'_{\rm e}t'_{\rm e}} - E_{m_{\rm e}l_{\rm e}t_{\rm e}}), \quad j = {\rm e}, \tag{23}$$

$$\omega_{\rm s} = \frac{1}{\hbar}(E_{m'_{\rm h}l'_{\rm h}t'_{\rm h}} - E_{m_{\rm h}l_{\rm h}t_{\rm h}}), \quad j = {\rm h}. \tag{24}$$

These frequency values correspond to conduction electron intersubband transitions or hole intersubband transitions in the valence band. By the scale problem, we have shown only a few transitions at all spectrums. Resonant electron transitions are indicated by $\Gamma_{\rm e}(m'_{\rm e}, t'_{\rm e}, l'_{\rm e}; m_{\rm e}, t_{\rm e}, l_{\rm e})$ and $\Gamma_{\rm h}(m_{\rm h}, t_{\rm h}, l_{\rm h}; m'_{\rm h}, t'_{\rm h}, l'_{\rm h})$ corresponding to conduction electrons or valence hole intersubband transitions, respectively. In these cases, the $\omega_{\rm s}$ values for which we find singularities do not depend on the incident radiation frequency $\omega_{\rm l}$ and only depend on the energy differences between the valence and conduction subbands.

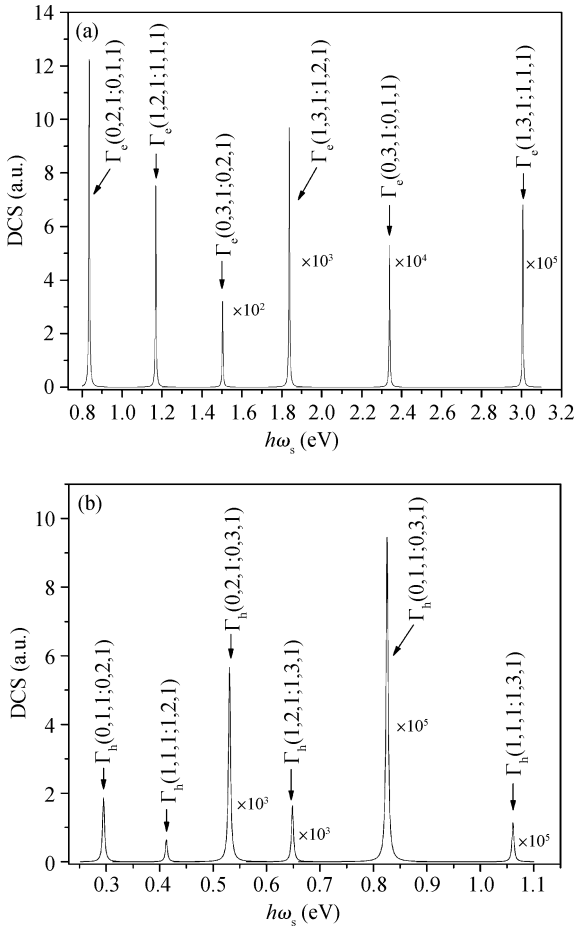

Fig. 2. Raman spectra of the CdS cylindrical QD in the scattering configuration $Z(\boldsymbol{e}_1, \boldsymbol{e}_{\rm sr})\overline{Z}$. The radius and thickness are 2.5 and 3.0 nm. (a) and (b) correspond to the process with the intermediate state in the conduction and valence bands, respectively.

In Fig. 1 we show the emission spectrum of the cylindrical QD in the scattering configuration $Z(\boldsymbol{e}_1, \boldsymbol{e}_{\rm sr})\overline{Z}$. The radius and thickness of the QD are 2.5 and 3.0 nm. From this figure, we find the following characteristics: (1) that the value of singularities due to the electron is larger than that due to the hole; (2) that the positions ($\hbar\omega_{\rm s}$) of the singularities corresponding to the valence hole intersubband transitions are smaller than those of the conduction electron intersubband transitions with the same quantum numbers (e.g. $\Gamma_{\rm h}(0,1,1;0,2,1)$ and $\Gamma_{\rm e}(0,2,1;0,1,1)$; $\Gamma_{\rm h}(1,1,1;1,2,1)$ and $\Gamma_{\rm e}(1,2,1;1,1,1)$, etc.). This characteristic tells us that the difference in energy levels between the valence hole subband is much smaller than that between the conduction electron subband in this system. The same results have been obtained in Refs. [12, 16]. (3) As the quantum number $m_{\rm e(h)}$ increases, the value of the singularities decreases. Further calculation reveals that when $m_{\rm e(h)} \to \infty$, the Raman intensity becomes very weak and can be ignored. So the main contributions to the DCS are those transitions with small $m_{\rm e(h)}$. This figure pro-

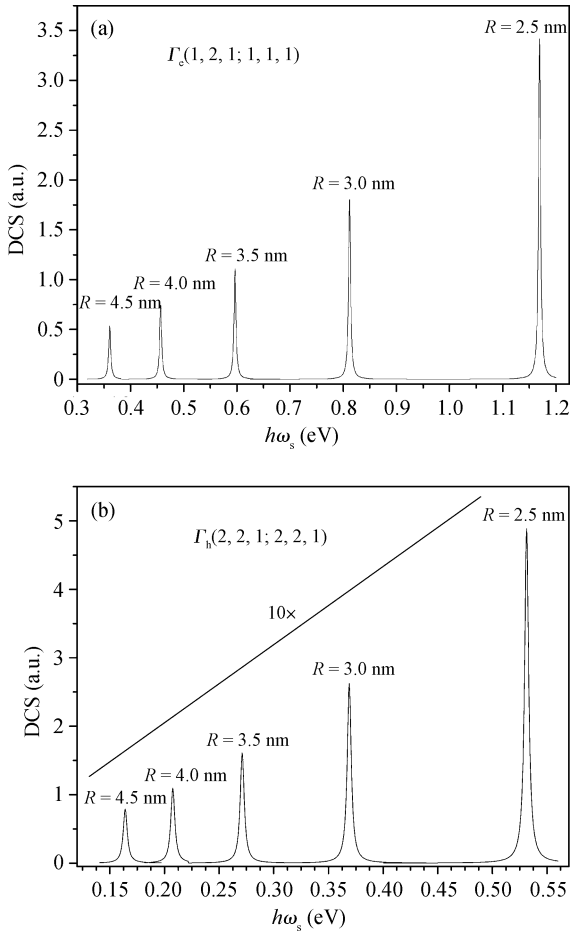

Fig. 3. Raman spectra of the CdS cylindrical QD with various radii. (a) and (b) correspond to the process with the intermediate state in the conduction and valence bands, respectively.

vides a transparent understanding of the electron subband energy structure of the cylindrical QD.

In Fig. 2 we show the emission spectra with transitions between higher energy level subbands. (a) and (b) correspond to the process with the intermediate state in the conduction and valence band, respectively. The radius and thickness of the QD are the same as Fig. 1. From this figure, it can be seen that with the same $m_{e(h)}$ (e.g. $m_{e(h)} = 0, 1$) the Raman intensity with transitions between large $t_{e(h)}$ is much weaker than that with transitions between small $t_{e(h)}$. As indicated in the figure, the contributions to the DCS for transitions $\Gamma_{e(h)}(0, 3, 1; 0, 1, 1)$, $\Gamma_{e(h)}(0, 3, 1; 0, 2, 1)$, $\Gamma_{e(h)}(1, 3, 1; 1, 1, 1)$ and $\Gamma_{e(h)}(1, 3, 1; 1, 2, 1)$ are 2–5 orders smaller than those for transitions $\Gamma_{e(h)}(0, 2, 1; 0, 1, 1)$, $\Gamma_{e(h)}(1, 2, 1; 1, 1, 1)$. For other transitions we get the same results. This investigation tells us that the transitions between small $t_{e(h)}$ make the main contributions to the DCS. When combined with Fig. 1, this gives us an important conclusion, that only transitions with small $m_{e(h)}$ and between small $t_{e(h)}$ make the main contributions to the DCS. Thus in the study of Raman scattering and many other cases, we should always consider the low energy level inter- or intra-subband transitions[13, 14, 21, 22]. For surface phonons in QDs, the inter-subband transitions can be neglected and the electrons are assumed to only occupy the ground subband[13, 14].

In Fig. 3, the emission spectrum for the different sizes of QD in the scattering configuration $Z(\boldsymbol{e}_1, \boldsymbol{e}_{sr})\overline{Z}$ is shown. The transitions we choose here are $\Gamma_e(1, 2, 1; 1, 1, 1)$ in Fig. 3(a) and $\Gamma_h(2, 1, 1; 2, 2, 1)$ in Fig. 3(b). The radii are shown in the figures. From this figure, we investigate that as R increases, the peaks shift to the lower energy. The reason for this is that as the width of the QD increases, the energy levels for both the electron and hole decrease. Moreover, as R decreases, the intensity of the peaks increases. This is caused by very anisotropic optical activity due to quantum confinement[17, 18]. As the radii decrease, the anisotropic optical activity becomes stronger due to more significant quantum confinement, so the intensity of the peaks corresponding to both the hole and electron increases.

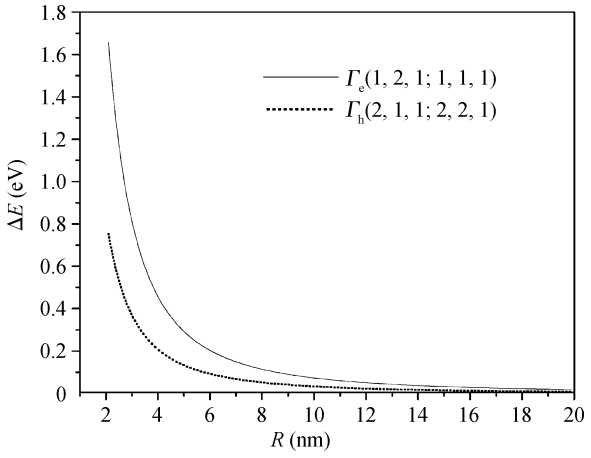

Fig. 4. The different energy levels $\triangle E$ between the two subbands for transitions $\Gamma_e(1, 2, 1; 1, 1, 1)$ and $\Gamma_h(2, 1, 1; 2, 2, 1)$ as a function of R.

In Fig. 4 we show the difference in energy levels (i.e. $\triangle E$) between the two subbands for transitions $\Gamma_e(1, 2, 1; 1, 1, 1)$ and $\Gamma_h(2, 1, 1; 2, 2, 1)$ as a function of the size of the QD. The solid line is for $\Gamma_e(1, 2, 1; 1, 1, 1)$ and the dotted line for $\Gamma_h(2, 1, 1; 2, 2, 1)$. As in the investigation by Raman scattering in Fig. 4, as the QD size increases,the $\triangle E$ decreases rapidly. When R is large enough, the $\triangle E$ will converge to zero. This reveals that when $R \to \infty$, the quantum confinement effect caused by R will disappear and the energy of the electrons and holes will become continuous. The QD will change into a two-dimensional QW.

5. Conclusion

In this work, we theoretically investigated the DCS for the ERS process associated with an electron and a hole in a CdS cylindrical QD structure. A rich spectrum, which is the main characteristic of the ERS, was obtained and interpreted. The results revealed that the contribution corresponding to the electron is larger than that due to the hole and for different QD sizes, and the DCS for both the electron and hole changes sensitively. The emission spectrum for the different sizes of QD reveals the anisotropic optical activity due to the quantum confinement of this system[17, 18]. Moreover, the investigation tells us that only transitions with small $m_{e(h)}$ and between small $t_{e(h)}$ make the main contributions to the DCS. The spectrum we get here could be used to study the electron band structures of such a system.

References

[1] Du J, Wang Q P, Balocco C, et al. Room-temperature operated and fully gate-bias controlled memory devices based on self-assembled InAs/GaAs quantum dots. Chinese Journal of Semiconductors, 2006, 27: 363

[2] Yang W F, Song X H, Gong S Q, et al. Carrier-envelope phase dependence of few-cycle ultrashort laser pulse propagation in a polar molecule medium. Phys Rev Lett, 2007, 99: 133602

[3] Deng N, Pan L Y, Liu Z H, et al. Low voltage flash memory cells using SiGe quantum dots for enhancing F–N tunneling. Chinese Journal of Semiconductors, 2006, 27: 451

[4] Arakawa Y, Sakaki H. Multidimensional quantum well laser and temperature dependence of its threshold current. Appl Phys Lett, 1982, 40: 939

[5] Niu Z C, Ni H Q, Fang Z D, et al. 1.3 μm InGaAs/InAs/GaAs self-assembled quantum dot laser diode grown by molecular beam epitaxy. Chinese Journal of Semiconductors, 2006, 27: 482

[6] Bimberg D, Grundmann M, Ledentsov N N. Quantum dot heterostructures. New York: John Wiley, 1999

[7] Wang D C, Zhang Y M, Zhang Y M, et al. Raman analysis of epitaxial graphene on 6H-SiC $(000\bar{1})$ substrates under low pressure environment. Journal of Semiconductors, 2011, 32: 113003

[8] Cardona M. Lattice vibrations in semiconductor superlattices. J Superlattices Microstruct, 1990, 7: 183

[9] Zhang G J, Xiu B, Chen Y H, et al. Raman scattering of InAs quantum dots with different deposition thicknesses. Chinese Journal of Semiconductors, 2006, 27: 1012

[10] Comas F, Trallero-Giner C, Perez-Alvarez R J. Interband-interband electronic Raman scattering in semiconductors. J Phys C, 1986, 19: 6479

[11] Bergues J M, Riera R, Comas F, et al. Electron Raman scattering in cylindrical quantum wires. J Phys: Condens Matter, 1995, 7: 7273

[12] Zhao X F, Liu C H. One phonon resonant Raman scattering in free-standing quantum wires. Phys Lett A, 2007, 364: 70

[13] Zhong Q H, Liu C H, Zhang Y Q, et al. One-phonon-assisted resonant electron Raman scattering of GaAs quantum dots in an AlAs matrix. Phys Lett A, 2008, 372: 2103

[14] Liu C H, Ma B K, Chen C Y. Surface optical phonon-assisted electron Raman scattering in a semiconductor quantum disc. Chin Phys B, 2002, 11: 7

[15] Menendez E, Trallero-Giner C, Cardona M. Vibrational resonant Raman scattering in spherical quantum dots: exciton effects. Phys Status Solidi B, 1997, 199: 81

[16] Maksym P, Chakraborty T. Quantum dots in a magnetic field: role of electron–electron interactions. Phys Rev Lett, 1990, 65: 108

[17] Dorigoni L, Bisi O, Bernardini F, et al. Electron states and luminescence transition in porous silicon. Phys Rev B, 1996, 53: 4557

[18] Ossicine S, Dorigoni S, Bisi O. Luminescence in porous silicon: the role of confinement and passivation. Appl Surf Sci, 1996, 102: 395

[19] Chernoutsan K, Dneprovskii V, Gavrilov S, et al. Linear and nonlinear optical properties of excitons in semiconductor C dielectric quantum wires. Physica E, 2002, 15: 111

[20] Chang K, Xia J B. Spatially separated excitons in quantum-dot quantum well structures. Phys Rev B, 1998, 57: 9780

[21] Xie H J, Chen C Y. Bound polaron in a cylindrical quantum wire of a polar crystal. Phys Rev B, 2000, 61: 4827

[22] Yoffe A D. Semiconductor quantum dots and related systems: electronic, optical, luminescence and related properties of low dimensional systems. Adv Phys, 2001, 50: 1